Journal of Power Sources 257 (2014) 138–146

Contents lists available at ScienceDirect

Journal of Power Sources

journal homepage: www.elsevier.com/locate/jpowsour

Electrocatalysis of carbon black- or poly(diallyldimethylammonium chloride)-functionalized activated carbon nanotubes-supported Pd–Tb towards methanol oxidation in alkaline media

Li Wang [a,b], Yi Wang [a,*], An Li [b], Yunshang Yang [b], Qinghu Tang [c], Hongbin Cao [a], Tao Qi [a], Changming Li [d]

[a] National Engineering Laboratory for Hydrometallurgical Cleaner Production Technology, Institute of Process Engineering, Chinese Academy of Sciences, Beijing 100190, China
[b] College of Petrochemical Technology, Lanzhou University of Technology, Lanzhou 730050, China
[c] School of Chemistry and Chemical Engineering, Key Laboratory of Green Chemical Media and Reactions, Ministry of Education, Henan Normal University, Xinxiang 453007, China
[d] Institute for Clean Energy & Advanced Materials, Southwest University, Chongqing 400715, China

HIGHLIGHTS

- The Pd–Tb/C catalysts with different Pd/Tb ratios were synthesized.
- 20%Pd–1%Tb/C has a higher catalytic activity than 20%Pd/C for methanol oxidation.
- The higher metallic Pd content caused by Tb contributes to the better activity.
- The 20%Pd–1%Tb/aCNTS-PDDA catalyst exhibits a better catalytic activity.
- PDDA improves the dispersion of alloy particles and further increases metallic Pd.

GRAPHICAL ABSTRACT

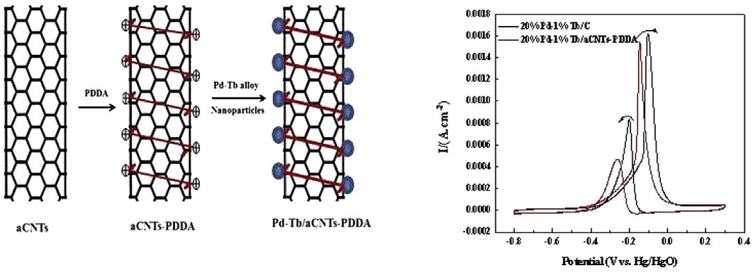

ARTICLE INFO

Article history:
Received 4 September 2013
Received in revised form
23 January 2014
Accepted 25 January 2014
Available online 2 February 2014

Keywords:
Pd–Tb/C
Electrocatalysts
Methanol oxidation
Activated carbon nanotubes
Poly(diallyldimethylammonium chloride)

ABSTRACT

The Pd–Tb/C catalysts with different Pd/Tb ratios were synthesized by a simple simultaneous reduction reaction with sodium borohydride in aqueous solution. The structure and morphology of those catalysts had been characterized by X-ray diffraction (XRD) and transmission electron microscopy (TEM). The electrocatalytic performance of those catalysts for methanol oxidation in alkaline media was investigated using cyclic voltammetry (CV), linear sweep voltammetry (LSV) and CO stripping experiments. It is found that the 20%Pd–1%Tb/C catalyst has a higher catalytic activity than the 20%Pd/C catalyst, but the effect of Tb cannot be explained by a bi-functional mechanism. According to the X-Ray photoelectron spectroscopy (XPS) analyses, it is suggested that the higher content of metallic Pd caused by the addition of Tb contributes to the better catalytic activity of 20%Pd–1%Tb/C. Based on the good electrocatalytic performance of 20%Pd–1%Tb/C, the 20%Pd–1%Tb catalyst supported on poly(diallyldimethylammonium chloride) (PDDA)-functionalized activated carbon nanotubes was prepared, and it exhibits a better catalytic activity. The improvement mainly results from the further increase of metallic Pd due to the presence of PDDA.

* Corresponding author. Tel.: +86 10 82544967; fax: +86 10 82544848 802.
E-mail address: wangyi@home.ipe.ac.cn (Y. Wang).

0378-7753/$ – see front matter © 2014 Elsevier B.V. All rights reserved.
http://dx.doi.org/10.1016/j.jpowsour.2014.01.109

1. Introduction

Direct methanol fuel cell (DMFC) has attracted enormous attention as a high-efficiently, low-emission future power source for portable electronic devices and fuel-cell vehicles, because of the facts that methanol is one of the most widely used fuels due to its low toxicity, abundance and availability at industrial scale compared to other alcohols [1–4]. But challenging issues such as methanol crossover, low catalytic activity of electrodes for both oxygen reduction reaction and methanol oxidation reaction, high costs of the Pt-based electrocatalysts and susceptibility of the catalysts to be poisoned by the CO-like intermediates formed in the methanol oxidation reaction are the main obstacles to commercialization of DMFC technology [5]. Thus, a lot of efforts have been made in the development of low-cost non-platinum electrocatalysts with comparable or improved kinetics for anodic methanol oxidation and better resistance to CO poisoning [6–10]. Recently, palladium has been demonstrated as an effective catalyst for the oxidation of both methanol and ethanol in alkaline media [11–14]. Moreover, Pd is cheaper and more abundant than Pt. However, the electrocatalytic activity of Pd for methanol oxidation in alkaline media is still needed to be enhanced [6].

Rare-earth metals combined with Pt or Pd have exhibited a number of promising characteristics in catalytic studies of methanol or ethanol electrooxidation over the past few years [15,16]. For example, Neto et al. [17] prepared Pt–rare earth/C electrocatalysts (rare earth = La, Ce, Pr, Nd, Sm, Tb, Dy, Ho and Er) for methanol oxidation by an alcohol reduction process using ethylene glycol as reduction agent and solvent and Vulcan XC-72 as support. They found that PtEr/C, PtTb/C, PtLa/C, PtNd/C and PtDy/C electrocatalysts showed superior performance for methanol oxidation at room temperature compared to Pt/C catalyst. Additionally, Tb has been investigated to promote the oxidation of ethanol with Pd/C in alkaline media, and it was found that Pd–Tb/C catalysts have higher catalytic activity, stability and lower activation energy for ethanol oxidation than Pd/C [18]. However, to the authors' knowledge, the catalytic performance of Pd–Tb/C bimetallic catalysts for methanol electrooxidation has not been reported yet. In this study, we prepared Pd/C electrocatalysts containing different amounts of Tb and investigated their activity for methanol electrooxidation in alkaline media.

It is well known that catalyst support has a significant influence on the catalytic activity. Carbon nanotubes (CNTs) are widely used as catalyst supports in fuel cells because of their high aspect ratio, high specific surface area, as well as unique structural, electronic and mechanical characteristics [19–21]. Some results showed that the CNTs-supported catalysts possess a higher catalytic activity than the conventional Vulcan XC-72 carbon black-supported catalysts [22–25]. Thus, in this work, a Pd–Tb catalyst supported on the multi-wall CNTs which were activated through alkali treatment was synthesized and its catalytic activity was investigated.

Recently, non-covalent functionalization is preferable for catalyst support applications, because it enables attachment of molecules or charged polyelectrolytes through π–π stacking or hydrophobic interactions, and thus preserves all the intrinsic electronic and structural properties of carbon materials [26,27]. This method is beneficial to the uniform dispersion of metal or alloy particles without detrimental effects on the electrical conductivity of catalysts. Furthermore, this functionalization can tailor the electronic solid state properties of metals or alloys, which could be propitious to the improvement of catalyst performance [28]. Poly(diallyldimethylammonium chloride) (PDDA) is an effective polyelectrolyte for non-covalent functionalization, and is commonly used in electrostatic assembling nanoparticles on CNTs surfaces [29]. Here, we functionalized the activated CNTs with PDDA. The results indicate that Pd–Tb nanoparticles deposited on the PDDA-functionalized CNTs have a significantly higher activity for methanol oxidation reaction compared to Pd–Tb electrocatalysts deposited on the carbon black and activated CNTs. This work provides a promising catalyst for DMFCs.

2. Experiment

2.1. Materials

Materials used in this work include sodium citrate ($Na_3C_6H_5O_7 \cdot 2H_2O$), palladium chloride, terbium nitrate ($Tb(NO_3)_3 \cdot xH_2O$), sodium borohydride ($NaBH_4$), methanol (CH_3OH), ethanol (C_2H_5OH), Nafion solution (5% in isopropanol and water), carbon black (XC-72, Gashub), deionized water, KOH and poly(diallyldimethylammonium chloride) (PDDA, 20 wt% in water, MW = 100,000–200,000, Aldrich–Sigma). The pristine multi-wall CNTs were supplied by Beijing Boyu High-Tech New Material Co. Ltd. All the chemicals were analytical grade.

2.2. Catalyst preparation

The short multi-wall CNTs (OD: 10–20 nm, ID: 5–10 nm, length: 0.5–2 μm, SSA: 233 $m^2\ g^{-1}$) were activated through alkali treatment [30]. Firstly, the activating agent (solid KOH) was mixed with the pristine CNTs in deionized water with a mass ratio of 5:1. After drying, the powder sample was treated at 750–800 °C with an Ar flow of 200 mL min^{-1} for 2 h. After activation, the sample was washed with dilute acid and deionized water to remove alkali compounds and impurities. In this study, the activated multi-wall CNTs were denoted as aCNTs, which were also used as catalyst support materials.

Poly(diallyldimethylammonium chloride) (PDDA)-functionalized aCNTs were prepared in a typical procedure. 100 mg aCNTs were put into a 250 mL beaker containing a PDDA solution (0.5 wt%, 100 mL), and then the suspension was stirred overnight. The final product was obtained through filtration and drying in a vacuum oven for 24 h. The functionalized aCNTs were denoted as aCNTs-PDDA.

To synthesize the electrocatalysts, stoichiometric support materials including carbon black, aCNTs and aCNTs-PDDA, respectively, were added into 50 mL deionized water and sonicated for 10 min. Then $PdCl_2$, $Tb(NO_3)_3 \cdot xH_2O$ and $Na_3C_6H_5O_7$ were added into the suspension and stirred for 15 min. Afterward, excess amounts of 0.01 M $NaBH_4$ (fresh prepared) were slowly dropped into the mixture, followed by stirring for 6 h at room temperature. Finally, the suspensions were filtered and washed several times with deionized water to completely remove all excess reducing agent. The remaining solids were dried in a vacuum oven at 60 °C. The final catalysts were denoted as Pd/C, Pd–Tb/C, Pd–Tb/aCNTs and Pd–Tb/aCNTs-PDDA, and the weight percentage of Pd is 20 wt% in these catalysts.

2.3. Physicochemical characterization

Structure and morphology of the catalysts were investigated using X-ray diffraction (XRD, X'Pert-PRO MPD, Cu K_α) and transmission electron microscopy (TEM, JEM-2100, 200 kV). The functional groups in the support materials were analyzed by Fourier transform infrared spectroscopy (FTIR, Bruker EQUINOX 55 Duroscope TM). The specific surface area, pore size and pore volume of the support materials were determined by analyzing the standard nitrogen adsorption isotherms measured with a pore and surface analyzer (Quantachrome Adsorb-1) at 77 K. The nature of surface species of catalysts was investigated by X-Ray photoelectron

spectroscopy (XPS, ESCALAB 250Xi (Thermo Fisher Scientific Inc.)). The elemental analysis was performed by Inductively Coupled Plasma Atomic Emission Spectrometry (ICP-AES, IRIS Intrepid II XSP (ThermoFisher)).

2.4. Electrochemical characterization

All the electrochemical measurements were conducted on an electrochemical workstation system (CHI760D, Chenhua, Shanghai) with a three-electrode cell using Pt foil and Hg/HgO (1 M KOH) electrode as the counter and reference electrodes, respectively. Cyclic voltammetry (CV) and linear sweep voltammetry (LSV) were performed in a 1 M KOH + 1 M CH_3OH solution, where oxygen was removed by purging N_2 for 15 min. To obtain the working electrode, 5 μL electrocatalyst ink was dropped onto the pretreated glassy carbon plate through a syringe. The ink was prepared by ultrasonically mixing 4 mg of electrocatalyst in 2 mL ethanol. Then, 1 μL of Nafion solution of 0.5 wt% in 2-propanol was dropped on top to fix the electrocatalyst. All potentials in the present study were given vs. Hg/HgO (1 M KOH) electrode. The CV and LSV tests were conducted at 50 and 20 mV s^{-1}, respectively, with potential ranging from −0.8 to 0.3 V. The LSV was measured at different temperatures. CO stripping was performed as follows: after purging the solution with N_2 for 20 min, gaseous CO was bubbled for 15 min to form CO adlayer on catalysts while maintaining potential at −0.8 V. Then excess CO in solution was purged with N_2 for 20 min and CO stripping voltammetry was recorded in 1 M KOH solution at 50 mV s^{-1}.

3. Results and discussion

3.1. Physical characterization and electrochemical performance of Pd–Tb supported on carbon black

Typical XRD patterns of the prepared catalysts with different ratios of Pd to Tb are shown in Fig. 1. The diffraction peak at ca. 25° in all the XRD patterns belongs to carbon black support. There are four diffraction peaks corresponding to (111), (200), (220) and (311) planes of the typical face-centered cubic structure of Pd at ca. 40°, 46°, 68° and 81°, respectively. No peak of Tb is observed, but according to the analysis of ICP-AES, the mass percentages of Pd and Tb in 20%Pd–1%Tb/C catalyst are 19.43 and 0.9360%, respectively, which are in close proximity to the theoretical values. This indicates that the Tb was either in an amorphous state, or alloyed with the Pd. It is notable that the addition of Tb caused clear shifts of the Pd peaks. For the catalysts with Tb ratios from 0.5% to 5%, the diffraction peaks at ca. 40° shift a little to higher 2θ value with respect to the corresponding peak in 20%Pd/C, which indicates that alloying had occurred. However, the peaks at ca. 40° in the patterns of the 20%Pd–10%Tb/C and 20%Pd–15%Tb/C catalysts shift a little to lower 2θ value compared to the 20%Pd/C catalyst. It is inferred that the intermetallic compound of Pd_3Tb may arise with the increase of Tb content because the most intense peak in the XRD pattern of Pd_3Tb is at ca. 38° (JCPDS 65-0738).

Fig. 2 presents the TEM images of the 20%Pd/C and 20%Pd–1% Tb/C catalysts. It can be seen that the nanoparticles are dispersed uniformly on the carbon black substrate with a little aggregation.

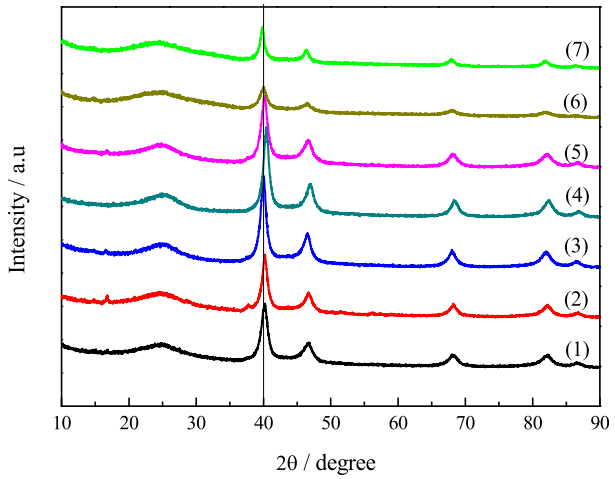

Fig. 1. XRD patterns of (1) 20%Pd/C (2) 20%Pd–0.5%Tb/C (3) 20%Pd–1%Tb/C (4) 20% Pd–2.5%Tb/C (5) 20%Pd–5%Tb/C (6) 20%Pd–10%Tb/C and (7) 20%Pd–15%Tb/C catalysts.

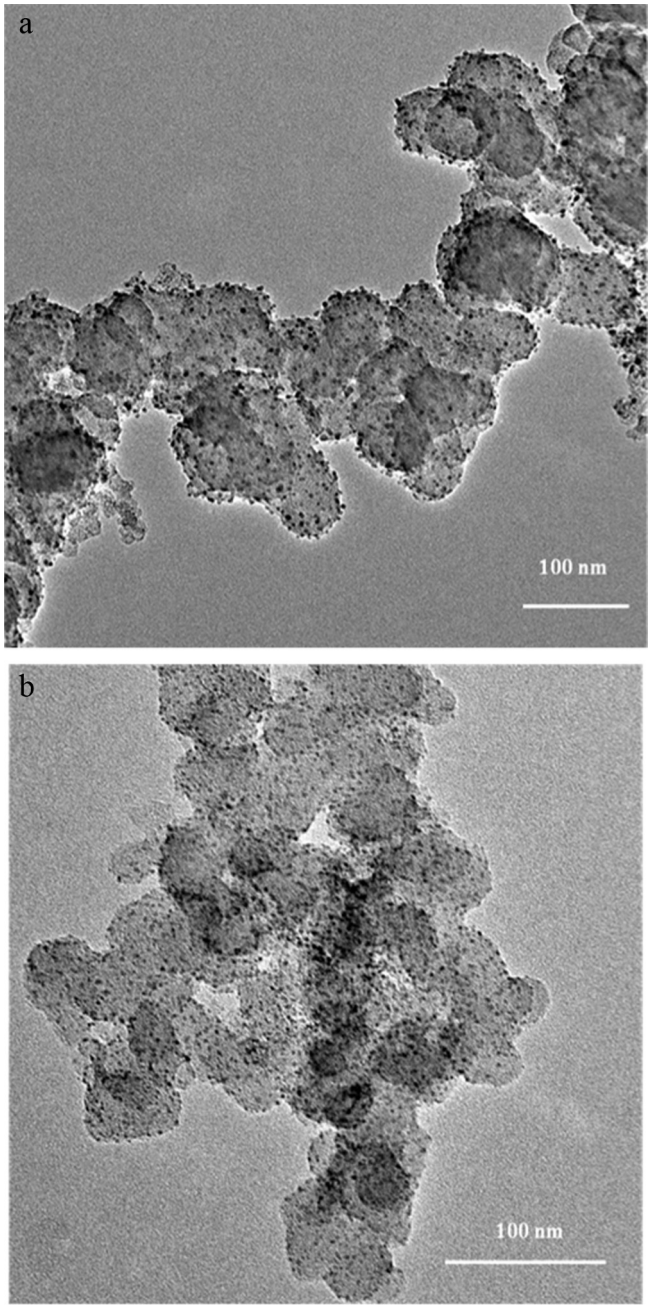

Fig. 2. TEM images of (a) 20%Pd/C and (b) 20%Pd–1%Tb/C.

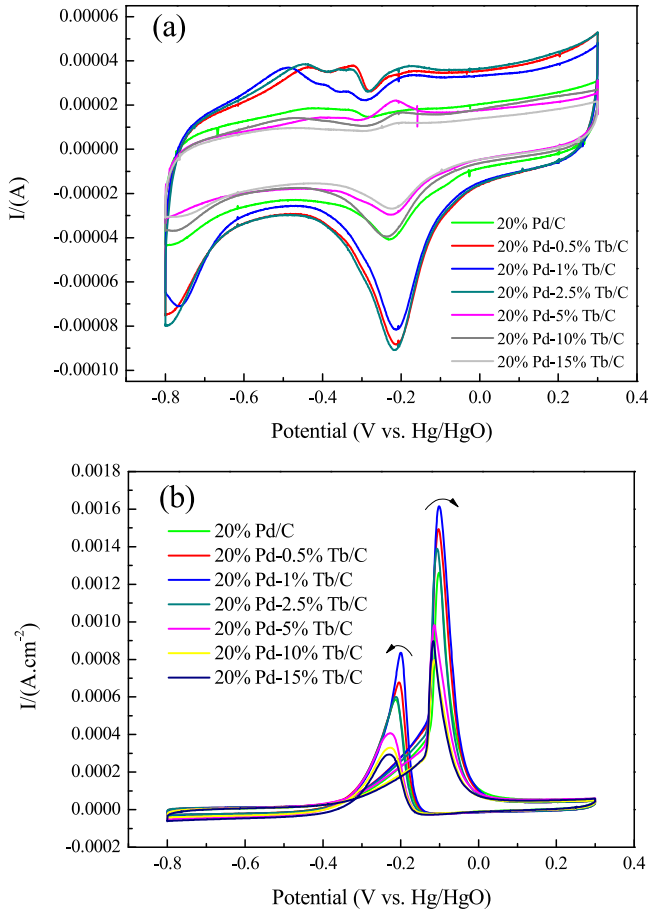

Fig. 3. Cyclic voltammograms of 20%Pd/C, 20%Pd–0.5%Tb/C, 20%Pd–1%Tb/C, 20%Pd–2.5%Tb/C, 20%Pd–5%Tb/C, 20%Pd–10%Tb/C, 20%Pd–15%Tb/C in (a) 1 M KOH and (b) 1 M KOH + 1 M CH_3OH solution, scan rate 50 mV s^{-1}.

The average sizes of metal or alloy particles in 20%Pd/C and 20%Pd–1%Tb/C are 3.352 and 2.734 nm, respectively.

Fig. 3(b) shows the CVs of methanol oxidation on the prepared catalysts which were performed in a 1 M KOH + 1 M CH_3OH solution. The results were normalized by the Pd electrochemical active surface area (ECSA) obtained from the CVs in the blank solution (Fig. 3(a)). Table 1 lists the specific ECSA values. It can be found that the specific ECSA values firstly increased with the addition of Tb, and then decreased with further increasing Tb content. This shows that the intermetallic compound of Pd_3Tb may have little electrochemical activity. As seen from Fig. 3(b), the methanol electrooxidation reaction on each electrode of the present investigation has been characterized by two well-defined anodic peaks: one in the forward (i.e., anodic condition) and the other one in the reverse scan. In the forward scan, the oxidation peak is corresponding to the oxidation of freshly chemisorbed species coming from methanol adsorption. In the reverse scan, the oxidation peak is primarily associated with removal of the partially oxidized carbonaceous species in the forward scan [31]. The onset potential and peak current densities of those electrodes are also listed in Table 1.

Table 1
Specific electrochemical active surface area, onset potential and peak current density of 20%Pd/C, 20%Pd–0.5%Tb/C, 20%Pd–1%Tb/C, 20%Pd–2.5%Tb/C, 20%Pd–5%Tb/C, 20%Pd–10%Tb/C and 20%Pd–15%Tb/C electrodes.

Samples	Pd specific electrochemical active surface area ($cm^2\ g^{-1}$ Pd)	Onset potential (V)	Peak current density (mA cm^{-2})
20%Pd/C	3.47×10^5	−0.47	1.266
20%Pd–0.5%Tb/C	5.98×10^5	−0.44	1.496
20%Pd–1%Tb/C	5.31×10^5	−0.50	1.614
20%Pd–2.5%Tb/C	6.04×10^5	−0.43	1.393
20%Pd–5%Tb/C	2.25×10^5	−0.46	0.984
20%Pd–10%Tb/C	2.77×10^5	−0.46	0.804
20%Pd–15%Tb/C	1.91×10^5	−0.46	0.891

As shown in Table 1, the onset potential of methanol oxidation on the 20%Pd–1%Tb/C catalyst is a little more negative than that on the other catalysts. Moreover, it can be found that the peak current density on the 20%Pd–1%Tb/C catalyst is the highest. It indicates that the 20%Pd–1%Tb/C catalyst has a better electrocatalytic activity for methanol oxidation, and the optimal content of Tb for improving methanol oxidation activity is 1%. Thus, we will limit our focus on the good performing catalyst 20%Pd–1%Tb/C.

To further demonstrate the excellent behavior of the 20%Pd–1% Tb/C catalyst, LSV tests were performed at several different temperatures on the 20%Pd/C and 20%Pd–1%Tb/C electrodes, and the results are shown in Fig. 4. It can be seen that the current densities increase with the rising of test temperatures.

Fig. 5 presents the relationship of the reciprocal of temperature and the logarithm of current density (at −0.10 V). An apparent activation energy value can be calculated according to Arrhenius equation [32]:

$$I = A \cdot e^{-E_a/RT} \quad (1)$$

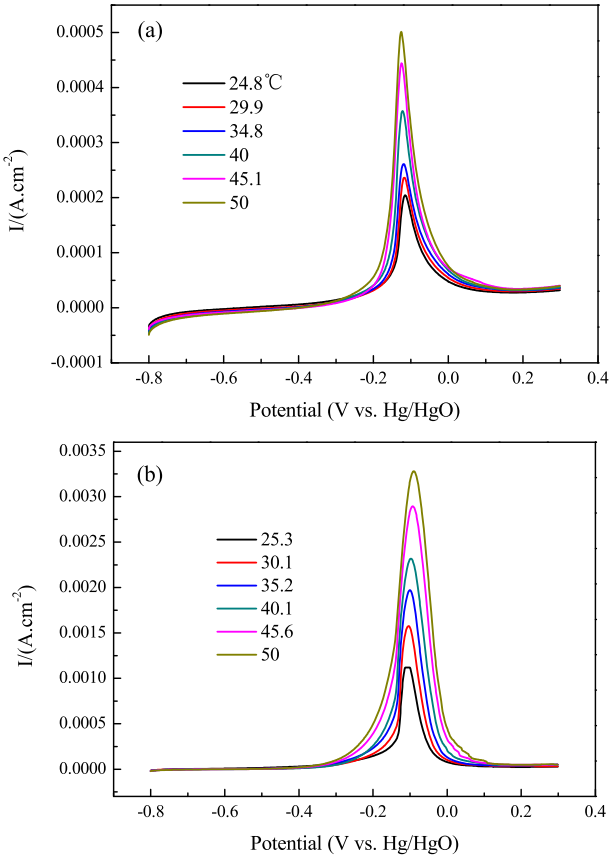

Fig. 4. LSV curves in 1 M KOH + 1 M CH_3OH solution at different temperatures for (a) 20%Pd/C and (b) 20%Pd–1%Tb/C, scan rate: 20 mV s^{-1}.

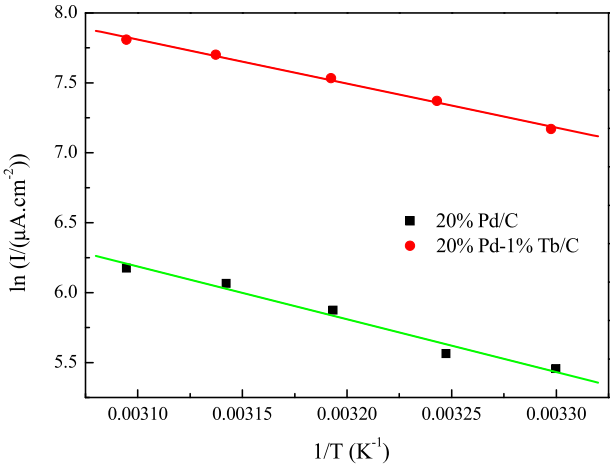

Fig. 5. The plot of ln I vs. $1/T$ (I: current density at −0.10 V; T: temperature in K).

where I is the current at a specific potential, R is the gas constant, T is the temperature in K and E_a stands for the apparent activation energy. By linearly fitting the relationship of ln I and $1/T$, it can be obtained that the E_a for 20%Pd/C and 20%Pd−1%Tb/C is 31.353 and 26.119 kJ mol^{-1}, respectively. It is obvious that the E_a of the 20%Pd−1%Tb/C catalyst is smaller than that of the 20%Pd/C catalyst. It indicates that, using the 20%Pd−1%Tb/C as electrocatalysts, the charge transfer process is faster. In short, an appropriate amount of Tb promotes the kinetics of the electrooxidation of methanol on Pd/C, and the difference of apparent activation energy further proves that 20%Pd−1%Tb/C has a higher catalytic activity than 20%Pd/C.

The promoting effect of the second metal is often explained by a bi-functional mechanism [6,33]. In other words, the second metal activates water at lower potentials than Pt or Pd and the activated water can oxidize the adsorbed CO or other poisoning intermediate and therefore liberate Pt or Pd active sites. To verify whether Tb promotes the removal of adsorbed CO by the bi-functional mechanism, CO stripping curves were collected, as shown in Fig. 6. It can be seen that the onset potential of CO oxidation on the 20%Pd−1%Tb/C catalyst is similar to that on the 20%Pd/C catalyst. This means that the addition of Tb does not facilitate the removal of CO or similar poisoning intermediate. Therefore, the promoting effect of Tb cannot be explained by a bi-functional mechanism.

To further investigate the function of Tb, Pd 3d core level spectra of the 20%Pd/C and 20%Pd−1%Tb/C catalysts were recorded in Fig. 7.

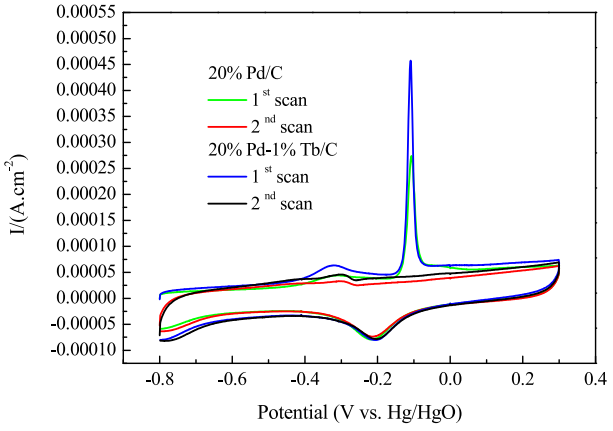

Fig. 6. CO stripping curves on the 20%Pd/C and 20%Pd−1%Tb/C catalysts recorded in 1 M KOH solution.

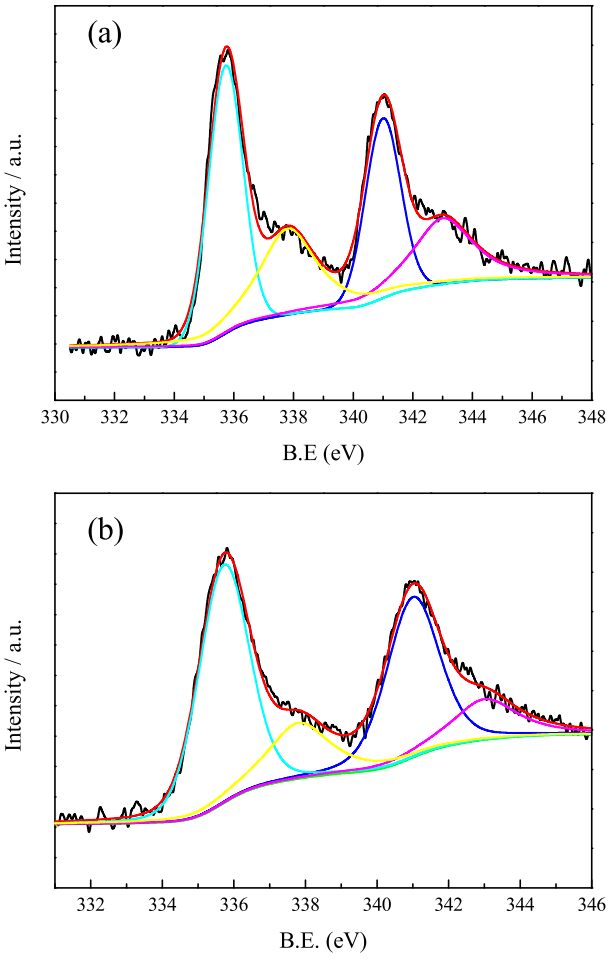

Fig. 7. XPS spectra of Pd (3d) for (a) 20%Pd/C and (b) 20%Pd−1%Tb/C catalysts (Fitting curves: Pd(0): cyan and blue; Pd(II): yellow and magenta). (For interpretation of the references to colour in this figure legend, the reader is referred to the web version of this article.)

The binding energies of all peaks are referenced to a C 1s value of 284.8 eV. The Pd 3d signals of 20%Pd/C were fitted by two pairs of overlapping Lorentzian curves (Fig. 7(a)). The more intense peaks (335.74 and 341.02 eV) are attributed to metallic palladium, Pd(0). The second set of doublets (337.86 and 343.08 eV) can be attributed to the Pd(II) chemical state on PdO or $Pd(OH)_2$. Fig. 7(b) presents the Pd 3d XPS spectra of the 20%Pd−1%Tb/C catalyst, which are similar to those of 20%Pd/C. However, the relative intensity of metallic Pd(0) in 20%Pd−1%Tb/C is 72.59%, higher than 56.02% obtained for 20%Pd/C. Table 2 lists the relative intensity of Pd(0) and Pd(II) of these two catalysts evaluated from XPS analyses. It indicates that the additional of Tb can increase the content of Pd(0) while decrease the content of Pd(II). In other words, Tb has a "metallization" effect on Pd. This may result from the difference of

Table 2
Binding energy (B.E.) and relative intensity of species from curve-fitted XPS spectra of Pd 3d.

Samples	B.E. of Pd $3d_{5/2}$/eV	B.E. of Pd $3d_{3/2}$/eV	Species	Relative intensity (%)
20%Pd/C	335.742	341.023	Pd(0)	56.02%
	337.860	343.075	Pd(II)	43.98%
20%Pd−1%Tb/C	335.785	341.057	Pd(0)	72.59%
	337.898	343.083	Pd(II)	27.41%

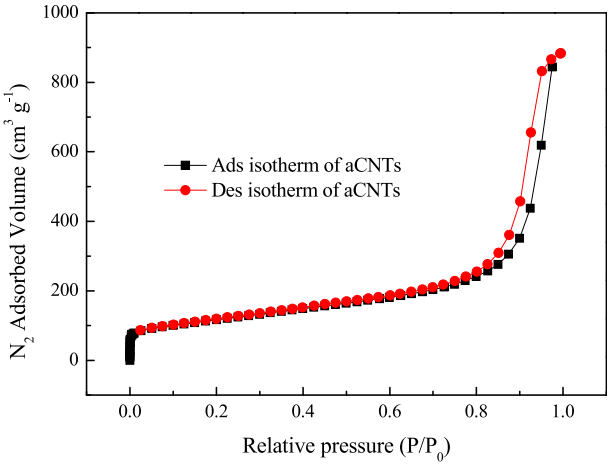

Fig. 8. Nitrogen isotherms measured for aCNTs at 77 K.

valence electron configuration between Tb and Pd. The valence electron configuration of the former is $4f^9 6s^2$, which has a trend to lose electrons. However, the latter has a valence electron configuration of $4d^{10}$, which contains unoccupied orbits. Thus, some electrons of Tb may have a trend to transfer to Pd, leading to an increase of metallic palladium. It is well known that the higher the content of metallic state in catalysts, the better the catalytic performance [28,34]. Therefore, the higher content of Pd(0) caused by the addition of Tb contributes to the better catalytic activity of the 20%Pd–1%Tb/C catalyst.

3.2. Physical characterization and electrochemical performance of Pd–Tb supported on activated CNTs

Based on the good electrocatalytic performance of the 20%Pd–1%Tb/C catalyst, the activated CNTs-supported 20%Pd–1%Tb catalyst was prepared and its catalytic activity was investigated. By alkali treatment for CNTs, a high specific surface area and big pore volume can be obtained [35]. In our study, nitrogen adsorption measurements were performed to characterize the change of the surficial and pore properties of carbon support materials. The nitrogen isotherms at 77 K were measured on aCNTs and the results are shown in Fig. 8. According to the analysis via BET equation, the specific surface area and pore volume are found to be

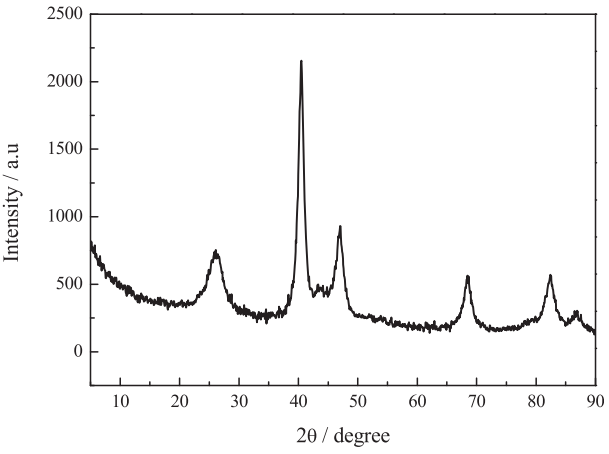

Fig. 9. XRD pattern of the 20%Pd–1%Tb/aCNTs catalyst.

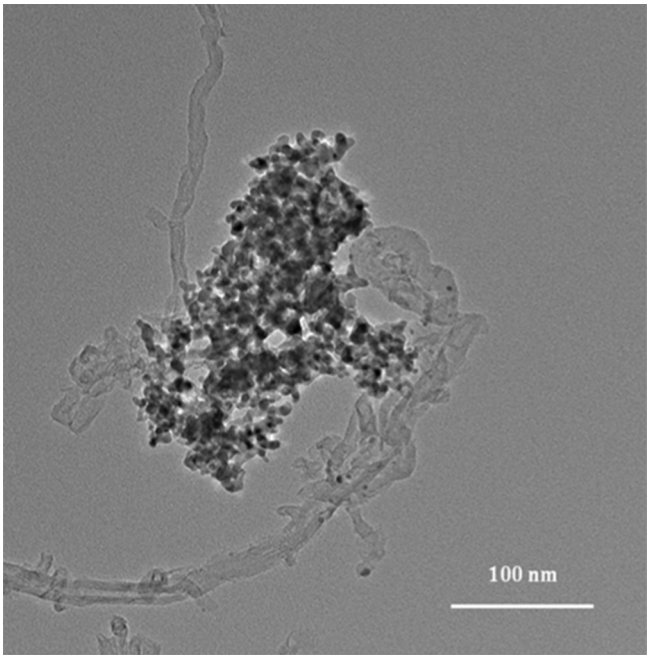

Fig. 10. TEM image of the 20%Pd–1%Tb/aCNTs catalyst.

461.651 $m^2\ g^{-1}$ and 0.958 $cm^3\ g^{-1}$, respectively. These values are about 1.8 and 2.8 times larger than those of carbon black (254.4 $m^2\ g^{-1}$ and 0.341 $cm^2\ g^{-1}$), respectively. A high specific surface area and big pore volume should be in favor of the increase of metal utilization and electrochemical activity. Thus, the aCNTs are considered to be a logical choice for an electrocatalyst support.

The XRD pattern of the 20%Pd–1%Tb/aCNTs catalyst is shown in Fig. 9. The diffraction peak at ca. 25° is attributed to the C (002) plane, proving the base is a carbon material. A few strong peaks of palladium are also clearly observed. No peak of Tb is observed, which is similar to the 20%Pd–1%Tb/C catalyst.

Typical TEM image of the 20%Pd–1%Tb/aCNTs catalyst is presented in Fig. 10. Compared to 20%Pd–1%Tb/C, the Pd–Tb particles supported on aCNTs have a significantly more serious degree of aggregation. Additionally, the average particle size in 20%Pd–1%Tb/aCNTs is 4.591 nm, which is bigger than that in 20%Pd–1%Tb/C. These results are contrary to the common rule because as a support material, a high specific surface area and large pore volume are

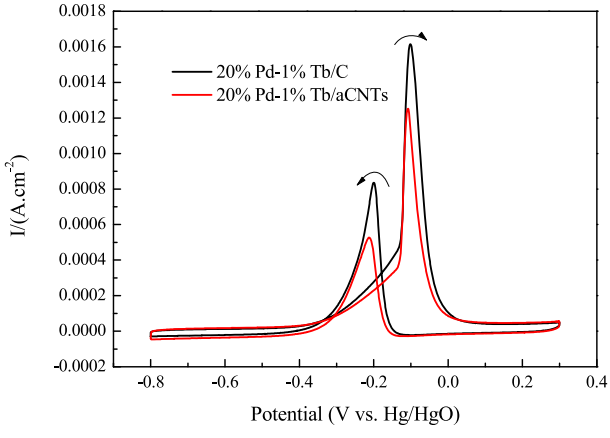

Fig. 11. CVs of the 20%Pd–1%Tb/C and 20%Pd–1%Tb/aCNTs catalysts in 1 M KOH + 1 M CH_3OH solution with a scan rate of 50 mV s^{-1}.

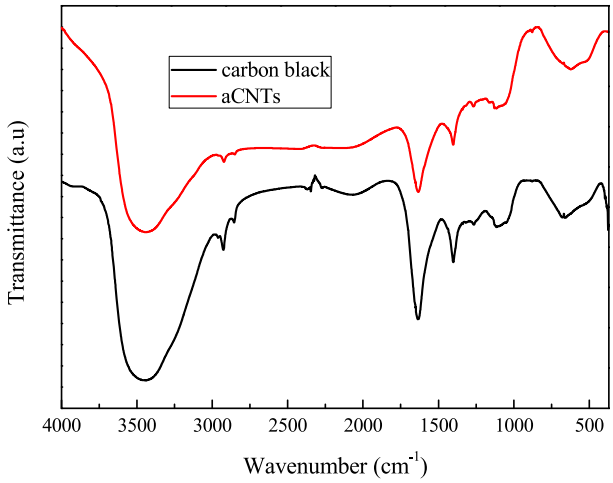

Fig. 12. FTIR spectra of carbon black and aCNTs.

usually beneficial to uniform distribution of metal or alloy particles with a smaller size [35]. The reason will be investigated in the following part.

The specific ECSA of 20%Pd–1%Tb/aCNTs obtained from the CVs in the blank solution was 2.45 × 10^5 cm^2 g^{-1} Pd, which is significantly smaller than that of 20%Pd–1%Tb/C (5.31 × 10^5 cm^2 g^{-1} Pd).

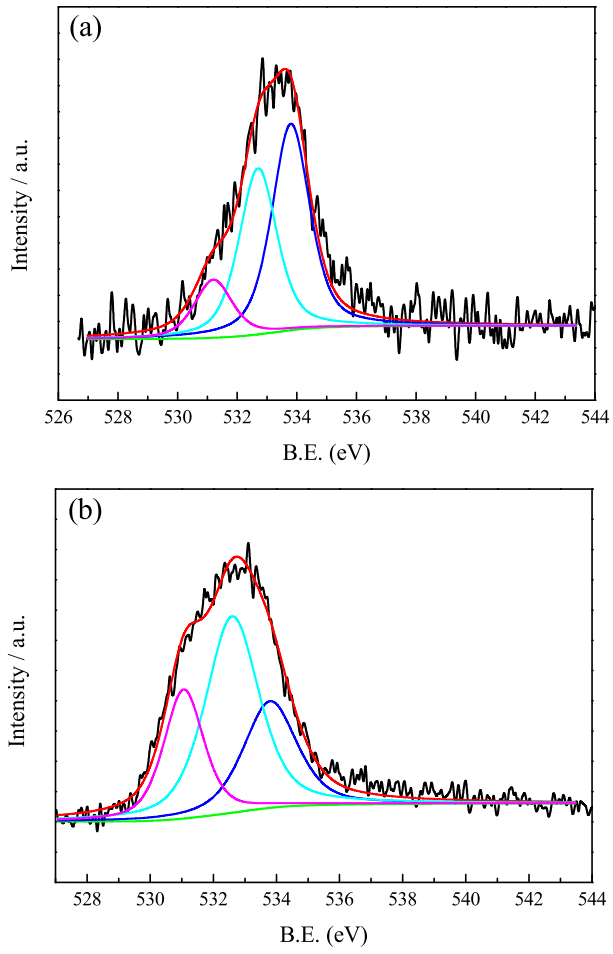

Fig. 13. O 1s XPS core level spectra of (a) carbon black and (b) aCNTs.

This results from the high aggregation degree of alloy particles in the former one. Fig. 11 shows the CVs of the 20%Pd–1%Tb/aCNTs electrocatalyst in a 1 M KOH + 1 M CH_3OH solution. For comparison, the CVs of 20%Pd–1%Tb/C are also shown in this figure. It is found that the onset potentials of both samples are similar, but the peak current density on 20%Pd–1%Tb/aCNTs is lower than that on 20%Pd–1%Tb/C. It indicates that the catalytic activity of the 20%Pd–1%Tb/aCNTs catalyst for methanol oxidation is worse than that of the 20%Pd–1%Tb/C catalyst. The deterioration of electrocatalytic performance of the catalyst supported on aCNTs is attributed to the high aggregation degree and big size of Pd–Tb particles, which decreases the metal utilization.

In order to investigate the reason for the high aggregation degree of alloy particles in the 20%Pd–1%Tb/aCNTs catalyst, the FTIR spectra and O 1s XPS spectra of the support materials (carbon black and aCNTs) were performed and shown in Figs. 12 and 13, respectively. From Fig. 12, it is seen that these two support materials show similar FTIR spectra. The absorption bands near 3445 cm^{-1} can be assigned to both hydroxyl groups and water, but the band in aCNTs becomes much weaker compared to that in carbon black, which indicates that the former one may possess less hydroxyl groups or/and be more hydrophobic. The bands near 1630 cm^{-1} originate from conjugated C=C bonds. Additional bands at 1400, 1250 and 1100 cm^{-1} are assigned to the bending vibration of C=C, epoxy C–O and C–O–C bonds, respectively. To compare the amounts of different oxygen-containing functional groups, the O 1s signals shown in Fig. 13 were fitted by three Lorentzian curves. The peaks at 533.8, 532.8 and 531.1 eV are attributed to –C–OH, –C–O–C– and epoxy C–O groups, respectively [36–38]. For carbon black, the relative intensity of -C-OH is 47.9%, and the total relative intensity of the other two groups is 52.1%. However, for aCNTs, these two percentages are 26.7 and 73.3%, respectively. In other words, aCNTs have less hydroxyl groups and more ether and epoxy groups compared to carbon black, which is consistent with the FTIR results. It is well known that hydroxyl groups are more hydrophilic than ether and epoxy groups. Thus, it is suggested that compared to carbon black, aCNTs are more hydrophobic, which may result in the worse dispersion of alloy particles.

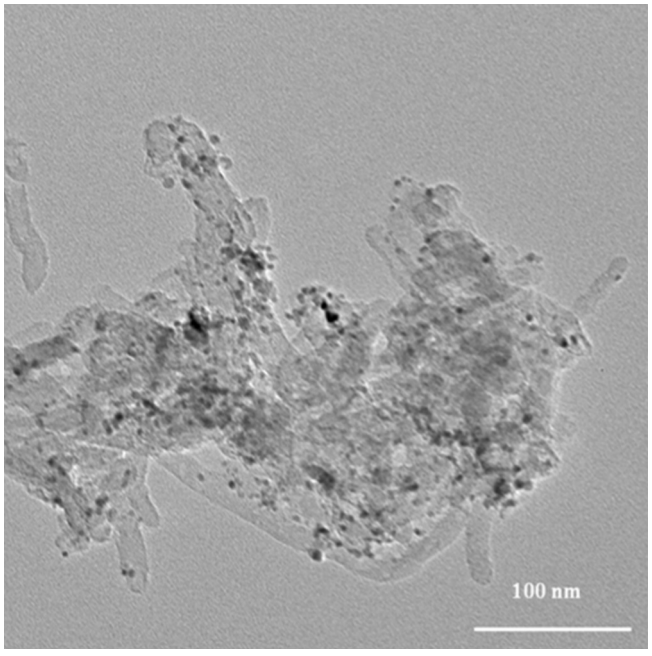

Fig. 14. TEM image of the 20%Pd–1%Tb/aCNTs-PDDA catalyst.

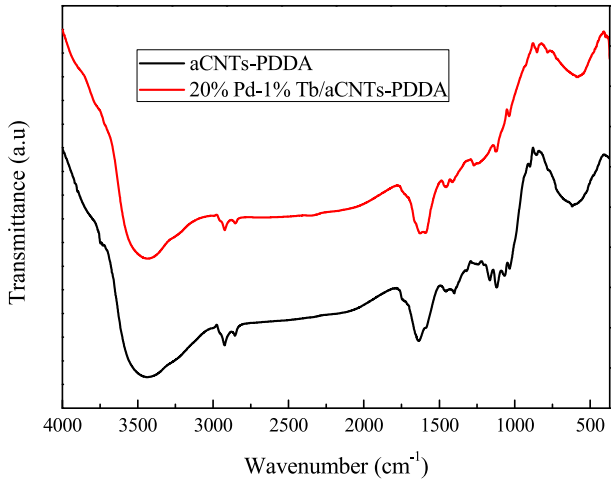

Fig. 15. FTIR spectra of aCNTs-PDDA and 20%Pd–1%Tb/aCNTs-PDDA.

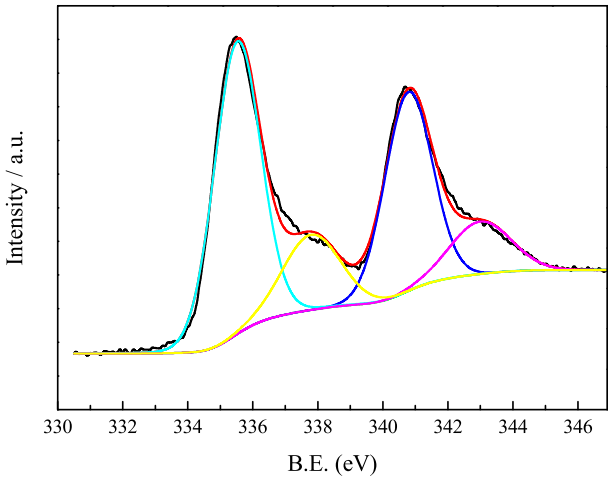

Fig. 17. XPS spectra of Pd (3d) for the 20%Pd–1%Tb/aCNTs-PDDA catalyst (Fitting curves: Pd(0): cyan and blue; Pd(II): yellow and magenta). (For interpretation of the references to colour in this figure legend, the reader is referred to the web version of this article.)

3.3. Physical characterization and electrochemical performance of Pd–Tb supported on PDDA-functionalized activated CNTs

To improve the dispersion status of alloy particles, the aCNTs were functionalized with PDDA. Fig. 14 shows the TEM image of the 20%Pd–1%Tb/aCNTs-PDDA catalyst. It is found that the Pd–Tb nanoparticles disperse significantly more uniformly compared to those loaded on aCNTs although there is still a little aggregation. The improvement of dispersion status results from the self-assembly process of nanoparticles on PDDA-functionalized aCNTs [26].

Fig. 15 presents the FTIR spectra of aCNTs-PDDA and 20%Pd–1% Tb/aCNTs-PDDA. Compared to the FTIR spectra of aCNTs (shown in Fig. 12), a small peak at ~1470 cm^{-1} and a shoulder peak near 1610 cm^{-1} appear. It has been reported [39,40] that the absorption band near 1635 cm^{-1} can be assigned to the ring vibration of the pyrrolidine structure in PDDA, but it will shift to 1610 cm^{-1} along with an intensity decrease of the peak at ~1470 cm^{-1} due to PDDA-aCNTs interaction. Thus, this indicates that the aCNTs were successfully functionalized by PDDA.

Fig. 16 displays the CVs of the 20%Pd–1%Tb/aCNTs-PDDA catalyst measured in a 1 M KOH + 1 M CH_3OH solution. For comparison, the CVs of the 20%Pd–1%Tb/C catalyst are also shown in this figure. It is clear that compared with 20%Pd–1%Tb/C, though the peak current density in the forward scan is similar, the onset potential and peak potential of 20%Pd–1%Tb/aCNTs-PDDA are more negative. Moreover, it can be found that the ratios of current density of the oxidation peak in the forward scan to the oxidation peak in the reverse scan are different between these two samples. For the catalyst supported on carbon black, the ratio is 1.93, while for the catalyst supported on aCNTs-PDDA, the ratio increases to 3.28. Usually, the larger the ratio is, the better the performance of the electrocatalyst may be. Because this anodic peak in the reverse scan is attributed to the removal of the incompletely oxidized carbonaceous species formed in the forward scan, and these carbonaceous species are mostly in the form of linearly bonded Pd=C=O [41], the larger ratio of current density of the anodic peak in the forward scan to the anodic peak in the reverse scan may show that the catalyst has a better electrocatalytic activity and resistance to CO poisoning [6]. In short, according to the CVs (Fig. 16), it is indicated that 20%Pd–1%Tb/aCNTs-PDDA has a better catalytic activity for methanol electrooxidation in alkaline media, which may result from the good dispersion of Pd–Tb nanoparticles on aCNTs-PDDA due to a self-assembly process [26].

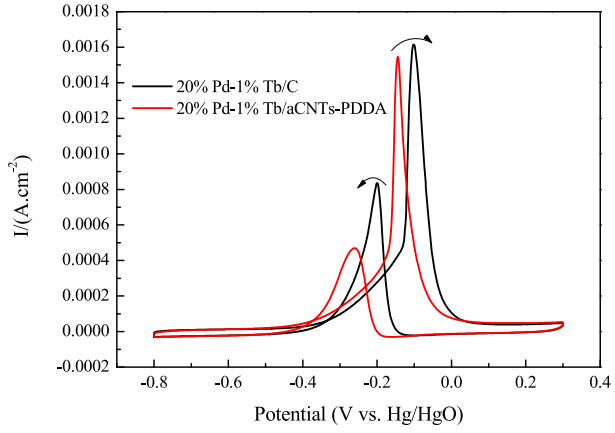

Fig. 16. CVs of the 20%Pd–1%Tb/C and 20%Pd–1%Tb/aCNTs-PDDA catalysts in 1 M KOH + 1 M CH_3OH solution with a scan rate of 50 mV s^{-1}.

To further understand the effect of PDDA, the nature of the surface species of 20%Pd–1%Tb/aCNTs-PDDA was investigated by XPS. Fig. 17 presents the Pd 3d spectra of this catalyst. It is seen that the XPS spectra are similar to those of the 20%Pd/C and 20%Pd–1% Tb/C catalysts (shown in Fig. 7). However, it is obtained by fitting that the content of Pd(0) and Pd(II) in 20%Pd–1%Tb/aCNTs-PDDA is 75.64 and 24.36%, respectively. In other words, the content of Pd(0) is higher than that in 20%Pd–1%Tb/C, which may be ascribed to the presence of PDDA. Because PDDA is a polycation, i.e., it is positively charged [26], an electrostatic inductive effect in the preparation process of the PDDA-functionalized aCNTs supported catalyst will lead to an increase in the content of metallic palladium [42]. The higher content of metallic state in catalysts will result in the better catalytic performance [28,34]. Therefore, it is suggested that besides improving the dispersion status of alloy particles, a "metallization" effect of PDDA on Pd also contributes to the better performance of the 20%Pd–1%Tb/aCNTs-PDDA catalyst.

4. Conclusions

In this study, the Pd–Tb/C catalysts with different amounts of terbium were prepared, and the catalytic performance towards methanol electrooxidation in alkaline media was investigated. It

was found that the 20%Pd–1%Tb/C catalyst has a higher activity than the 20%Pd/C catalyst, but this cannot be explained by a bi-functional mechanism. The analysis for XPS spectra indicates that the higher content of metallic Pd caused by the addition of Tb contributes to the better catalytic activity of 20%Pd–1%Tb/C. Based on the good electrocatalytic performance of the 20%Pd–1%Tb/C catalyst, the 20%Pd–1%Tb catalyst supported on activated carbon nanotubes was synthesized, but its electrocatalytic activity deteriorated, which is ascribed to the high aggregation degree of alloy particles due to the hydrophobicity of aCNTs. After aCNTs was functionalized by PDDA, the 20%Pd–1%Tb/aCNTs-PDDA catalyst exhibited a better catalytic activity than the 20%Pd–1%Tb/C catalyst. The improvement is attributed to the good dispersion status of alloy particles and the further increase of metallic Pd due to the presence of PDDA.

Acknowledgments

The authors are grateful for the financial support by One Hundred Talent Program of Chinese Academy of Sciences, as well as by the NSFC (51302264) of China.

References

[1] W.Z. Li, X. Wang, Z.W. Chen, M. Waje, Y.S. Yan, J. Phys. Chem. B 110 (2006) 15353–15358.
[2] Y.W. Zhang, G.H. Chang, S. Liu, J.Q. Tian, L. Wang, W.B. Lu, X.Y. Qin, X.P. Sun, Catal. Sci. Technol. 1 (2011) 1636–1640.
[3] R. Awasthi, R.N. Singh, Carbon 51 (2013) 282–289.
[4] S.Y. Shen, T.S. Zhao, J.B. Xu, Y.S. Li, J. Power Sources 195 (2010) 1001–1006.
[5] Z.L. Liu, X.H. Zhang, L. Hong, Electrochem. Commun. 11 (2009) 925–928.
[6] Y. Wang, X. Wang, C.M. Li, Appl. Catal. B 99 (2010) 229–234.
[7] Z.P. Sun, X.G. Zhang, R.L. Liu, Y.Y. Liang, H.L. Li, J. Power Sources 185 (2008) 801–806.
[8] Y. Zhao, X. Yang, J. Tian, F. Wang, L. Zhan, Int. J. Hydrogen Energy 35 (2010) 3249–3257.
[9] Y.J. Hu, P. Wu, Y.J. Yin, H. Zhang, C.X. Cai, Appl. Catal. B 111–112 (2012) 208–217.
[10] Y.Y. Jiang, Y.Z. Lu, F.G. Li, T.S. Wu, L. Niu, W. Chen, Electrochem. Commun. 19 (2012) 21–24.
[11] S.T. Nguyen, N. Kristian, S.Y. Wang, S.H. Chan, X. Wang, Appl. Catal. B 91 (2009) 507–515.
[12] J.D. Cai, Y.Y. Huang, Y.L. Guo, Electrochim. Acta 99 (2013) 22–29.
[13] E. Antolini, Energy Environ. Sci. 2 (2009) 915–931.
[14] H.T. Zheng, Y.L. Li, S.X. Chen, P.K. Shen, J. Power Sources 163 (2006) 371–375.
[15] E. Antolini, J. Perez, Int. J. Hydrogen Energy 36 (2011) 15752–15765.
[16] V. Raghuveer, K.R. Thampi, N. Xanthopoulos, H.J. Mathieu, B. Viswanathan, Solid State Ionics 140 (2001) 263–274.
[17] A.O. Neto, A.Y. Watanabe, M. Brandalise, M.M. Tusi, R.M.de S. Rodrigues, M. Linardi, E.V. Spinacé, C.A.L.G.O. Forbicini, J. Alloys Compd. 476 (2009) 288–291.
[18] S.T. Nguyen, D.S.L. Tan, J.M. Lee, S.H. Chan, J.Y. Wang, X. Wang, Int. J. Hydrogen Energy 36 (2011) 9645–9652.
[19] C.F. Zhou, S. Kumar, C.D. Doyle, J.M. Tour, Chem. Mater. 17 (2005) 1997–2002.
[20] L.M. Ang, T.S.A. Hor, G.Q. Xu, C.H. Tung, S.P. Zhao, J.L.S. Wang, Carbon 38 (2000) 363–372.
[21] H.T. Gomes, P.V. Samant, Ph. Serp, Ph. Kalck, J.L. Figueiredo, J.L. Faria, Appl. Catal. B 54 (2004) 175–182.
[22] E. Yoo, T. Okada, T. Kizuka, J. Nakamur, J. Power Sources 180 (2008) 221–226.
[23] D. Yang, C.M. Shen, X.J. Lu, H. Tong, J.J. Zhu, X.G. Zhang, H.J. Gao, Electrochim. Acta 62 (2012) 242–249.
[24] H. Shi, Electrochim. Acta 41 (1996) 1633–1639.
[25] S.C. Roy, P.A. Christiensen, A. Hamnett, K.M. Thomas, V. Trapp, J. Electrochem. Soc. 143 (1996) 3073–3079.
[26] S.Y. Wang, X. Wang, S.P. Jiang, Phys. Chem. Chem. Phys. 13 (2011) 6883–6891.
[27] S.Y. Wang, X. Wang, S.P. Jiang, Langmuir 24 (2008) 10505–10512.
[28] Z.M. Cui, C.M. Lia, S.P. Jiang, Phys. Chem. Chem. Phys. 13 (2011) 16349–16357.
[29] J.S. Wang, J.Y. Xi, Y.X. Bai, Y. Shen, J. Sun, L.Q. Chen, W.T. Zhu, X.P. Qiu, J. Power Sources 164 (2007) 555–560.
[30] Y. Wang, W.Q. Deng, X.W. Liu, X. Wang, Int. J. Hydrogen Energy 34 (2009) 1437–1443.
[31] M.Y. Li, S.Z. Zhao, G.Y. Han, B.S. Yang, J. Power Sources 191 (2009) 351–365.
[32] J.L. Cohen, D.J. Volpe, H.D. Abruna, Phys. Chem. Chem. Phys. 9 (2007) 49–77.
[33] X.Z. Yuan, H.J. Wang, J. Electroanal. Chem. 563 (2004) 81–89.
[34] W.L. Qu, Z.B. Wang, Z.Z. Jiang, D.M. Gu, G.P. Yin, RSC Adv. 2 (2012) 344–350.
[35] X. Sun, J.P. He, J. Tang, T. Wang, Y.X. Guo, H.R. Xue, G.X. Li, Y.O. Ma, J. Mater. Chem. 22 (2012) 10900–10910.
[36] H.L. Liu, Y. Wang, X.L. Gou, T. Qi, J. Yang, Y.L. Ding, Mater. Sci. Eng. B 178 (2013) 293–298.
[37] G.P. López, D.G. Castner, B.D. Ratner, Surf. Interface Anal. 17 (2004) 267–272.
[38] Z. Wang, E. Han, F. Liu, W. Ke, Corrosion 66 (2010) 075001–075009.
[39] P. Muthirulana, R. Velmurugan, Colloids Surf. B 83 (2011) 347–354.
[40] D.Q. Yang, J.F. Rochette, E. Sacher, J. Phys. Chem. B 109 (2005) 4481–4484.
[41] R. Manohara, J.B. Goodenough, J. Mater. Chem. 2 (1992) 875–887.
[42] Y. Wang, H.L. Liu, L. Wang, H.B. Wang, X. Du, F. Wang, T. Qi, J.M. Lee, X. Wang, J. Mater. Chem. A 1 (2013) 6839–6848.